Growth mechanisms and properties of 90° grain boundaries in $YBa_2Cu_3O_7$ thin films

C. B. Eom,* A. F. Marshall, Y. Suzuki, and T. H. Geballe
Department of Applied Physics and Center for Materials Research, Stanford University, Stanford, California 94305

B. Boyer and R. F. W. Pease
Department of Applied Physics and Department of Electrical Engineering, Stanford University, Stanford, California 94305

R. B. van Dover and Julia M. Phillips
AT&T Bell Laboratories, Murray Hill, New Jersey 07974

(Received 22 April 1992)

The transport properties of three types of 90° grain boundaries of (103) oriented $YBa_2Cu_3O_7$ (YBCO) thin films grown epitaxially on (101) $SrTiO_3$ and (101) $LaAlO_3$ substrates *in situ* by 90° off-axis sputtering are compared. A simple description of the in-plane crystallographic film orientation is given by substrate [010]||YBCO[010] and substrate [$\bar{1}$01]||YBCO ⟨301⟩. A domain structure exists with the CuO_2 planes oriented at ±45° to the substrate surface (i.e., parallel to the substrate [010] direction). Therefore, specific sets of 90° grain boundaries are observed in both principal in-plane directions. The normal-state conductivity and the critical current density of these films along the YBCO [010] direction are as high as the best quality *c*-axis films, which have no high-angle grain boundaries. The normal-state conductivity and critical current density along the ⟨301⟩ direction are much lower than in the [010] direction. However, the normalized magnetic-field dependence of J_c for both those directions is similar and shows no evidence of weak link behavior. These results have important implications for understanding the behavior of step-edge Josephson junctions. The anisotropic transport behavior in the normal and superconducting state is explained by the microstructure and a simple transport model.

I. INTRODUCTION

Due to the anisotropic crystal structure of high-T_c superconductors, many superconducting and normal state properties are also very anisotropic. Considerable effort has been devoted to measurements along different directions to explore the extent of the anisotropy. Tozer *et al.*[1] and Worthington *et al.*[2] measured several anisotropic properties of $YBa_2Cu_3O_7$ (YBCO) single crystals such as resistivity, critical current density, H_{c2}, superconducting coherence length, etc. Difficulties in synthesizing single crystals larger than a few hundred microns, however, have made such experiments hard to perform. Additionally, the quality of the crystals varies, because it is difficult to obtain uniform oxygen concentration in single crystals.

On the other hand, it is easy to make uniform epitaxial thin films with the desired dimensions. Most films naturally grow with their *c* axis normal to the substate under typical growth conditions. This permits transport measurements along the *a-b* plane but not along the *c* direction. Recently, high quality *a*-axis oriented films were grown at Stanford[3] and Bellcore.[4] Unfortunately, these *a*-axis films have two types of *b-c* domains which forbid one from measuring solely along the *c*-axis direction.

Several groups have reported (110) and/or (103) YBCO film growth on (110) $SrTiO_3$ substrates (see Ref. 5). Terashima *et al.*[6] found that a (110) oriented film was obtained for substrate temperatures around 530 °C, but a (103) orientation when grown above 600 °C. The surface of a (110) $SrTiO_3$ substrate is a rectangular lattice. This forces alignment of the CuO_2 planes in a specific direction. For a (110) oriented film, the CuO_2 planes are perpendicular to the $SrTiO_3$ [001] direction. On the other hand, in (103) oriented films the CuO_2 planes are always parallel to the $SrTiO_3$ [001] direction.

In a pure (110) oriented film, the two in-plane orthogonal directions are YBCO [$\bar{1}$10]|| substrate [$\bar{1}$10] and YBCO[001] || substrate [001]. This means that when the transport properties are measured along the substrate [001] direction, the current is flowing only along the YBCO *c*-axis direction. Hence, the anisotropy can be directly measured. Unfortunately, the intrinsic anisotropy is not measured in these (110) oriented YBCO films because the low growth temperature creates so many defects. In fact, all the properties are inferior in these films. In addition, Olsson *et al.*[7] recently reported that they observed cracks along the [001] direction of these types of YBCO films. They attributed the cause of these cracks to the different thermal expansion coefficients of YBCO along its *c* axis and $SrTiO_3$ along its [001] direction. Thus, (110) YBCO films have proven impractical for measurements of the intrinsic anisotropy.

Another choice to measure the anisotropic properties of YBCO is (103) oriented films. As we discuss below, higher growth temperatures have enabled us to make such films with far fewer defects than (110) films. Hence, there is the possibility of measuring the intrinsic anisotropy. The major drawback with (103) films compared to (110) films is that the anisotropy is not in a simple direction. Recently, Wada[8,9] and Kwo[10] have reported the growth of single domain (103) Bi-Sr-Ca-Cu-O and $La_{2-x}Sr_xCuO_4$ thin films, respectively. However, our (103) YBCO films, where the lattice parameter $c_0 \sim 3b_0$, do not grow as a single crystal or with a single in-plane orientation. Therefore, many types of grain boundaries

form in the films.

These are all 90° boundaries with respect to the c axis and are likely to be coherent, similar to previously studied a-axis films,[3,11] and in contrast to the lower angle grain boundaries studied by Dimos *et al.*[12] and more recently by Ivanov *et al.*[13] They have shown that the transport properties of certain twist and tilt boundaries degrade as the misorientation angle increases, suggesting that high angle grain boundaries are generally deleterious. Their work was carried out, respectively, on single grain boundaries of films deposited on $SrTiO_3$ bicrystals and on YSZ bicrystals. The misorientation angle between two crystals was varied from 0 to 45°. The J_c dropped 2 orders of magnitude when the misorientation angle was greater than 10°. However, it is not possible to make 90° grain boundaries using the bicrystal technique because the substrate is cubic.

Recently, Babcock *et al.*[14] reported weak-link-free behavior at high magnetic fields in a flux-grown YBCO bicrystal which contained two kinds of boundaries. One was a 90° [010] twist boundary (type A) and the other was a 90° [010] basal-plane-faced tilt boundary (type B)—see Fig. 4. They were not able to distinguish between the characteristics of the two boundaries which were electrically in parallel. The conclusion of weak-link-free behavior was based on the fact that the J_c across the boundary, $\sim 3\times 10^3$ A/cm^2 at 73 K, was not lower than the intragrain J_c, and on the features of the J_c vs H and I-V characteristics. However, for technological purposes it is desirable to measure weak link behavior in the range of 10^4 A/cm^2 to 10^6 A/cm^2. The intragrain J_c of highly textured thin films along the CuO_2 planes is close to the depairing critical current; therefore these films are ideal for studying weak-link behavior across grain boundaries.

We already reported the absence of weak-link behavior across the 90° [010] twist boundaries in (103) oriented YBCO thin films.[15] In this paper we discuss in detail the growth mechanisms, microstructures, and DC transport properties of (103) films. We make a comprehensive comparison of different types of 90° c-axis grain boundaries occurring in these films. Similar grain boundaries are present in step-edge junctions exhibiting weak-link-like behavior.[16–18] However, from our measurements of magnetic field dependence of J_c, we infer that this weak-link behavior is not simply due to the misorientation across the boundary as has been assumed. None of the 90° c-axis boundaries occurring in the (103) films show the strong dependence of critical current upon field found in step-edge junctions.

II. SYNTHESIS

The films we will discuss here were grown *in situ* by a single target, 90° off-axis sputtering technique.[19,20] Both (101) $SrTiO_3$ and (101) $LaAlO_3$ substrates have been used. We define the substrates as having a (101) orientation instead of the equivalent (110) for clarity. The directions of the substrate edges are [010] and [$\bar{1}$01]. On the (101) $LaAlO_3$ substrates, twin features cause visible lines aligned along the [010] direction. However, the (101) $SrTiO_3$ substrates require either the Laue technique or off-axis x-ray scans to identify the in-plane direction.

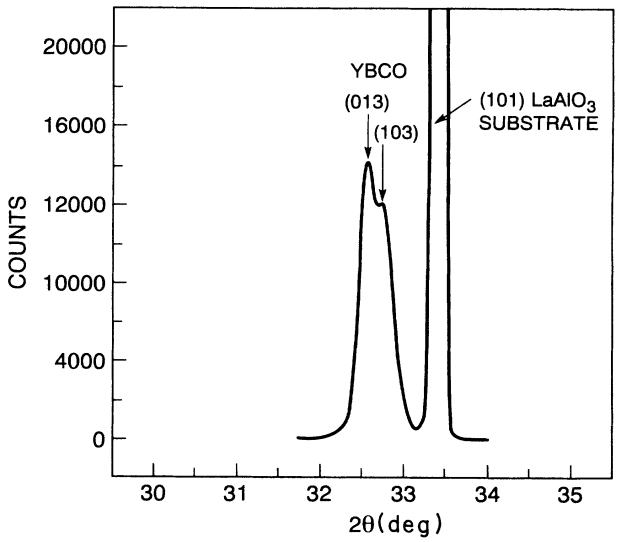

FIG. 1. X-ray diffraction θ–2θ scans on (103) YBCO thin film on (101) $LaAlO_3$.

The sputtering atmosphere consisted of 40 mTorr O_2 and 60 mTorr Ar. The rf power on the sputter gun (125 W) generated a self-bias of 50 V. The substrate block temperature was held at 720 °C. We simultaneously grew c-axis films on (100) MgO and (100) $SrTiO_3$ substrates to compare properties. After deposition, the chamber was immediately vented in O_2 until a pressure of 600 Torr was reached, and was then allowed to cool down. We deposited films with thicknesses from 660 to 4000 Å; because the (103) films have very rough surfaces we use the thickness of the adjacent c-axis films to define a "nominal" thickness for the (103) films.

III. STRUCTURAL PROPERTIES

A. Texture

The film textures were investigated by x-ray diffraction using a 4-circle diffractometer with a Cu $K\alpha$ source. Figure 1 shows the θ-2θ scan of a YBCO film grown on (101) $LaAlO_3$. The only peaks due to YBCO are the (103) and (013); however, these two peaks cannot be completely resolved by the instrument resolution. In a similar scan for a film grown on a (101) $SrTiO_3$ substrate, we were not able to identify a (013) peak because the strong (101) substrate peak overlaps it. The absence of any (110) oriented YBCO grains on either substrate was verified by off-axis scans of the (102) peak. The observation of both the (103) and (013) lines indicates the presence of (110) twins in the film due to the orthorhombic-to-tetragonal phase transformation during cooling. The mosaic spread in the (103) films is very anisotropic; rocking curve widths of the (103) and (013) reflections along the substrate [010] and [$\bar{1}$01] directions are 0.8° and 2.8°, respectively, both of which are bigger than that of either a good c-axis film[20] or a-axis film.[21] It is known, however, that if the rocking curve width of a c-axis film is less than about 3 degrees, then the DC normal state and superconducting proper-

ties are not affected.[22]

The in-plane texture was also investigated by off-axis scans of the (005) peak. It was confirmed that both the (103) and ($\bar{1}03$) variants [as well as (013) and (0$\bar{1}$3)] are present. The orientation of the CuO_2 planes changes by 90° between these two variants. It was confirmed that $SrTiO_3$[010]||YBCO[010], [100] and $SrTiO_3$[$\bar{1}$01] ||YBCO ⟨301⟩, ⟨031⟩. Therefore, all the CuO_2 planes

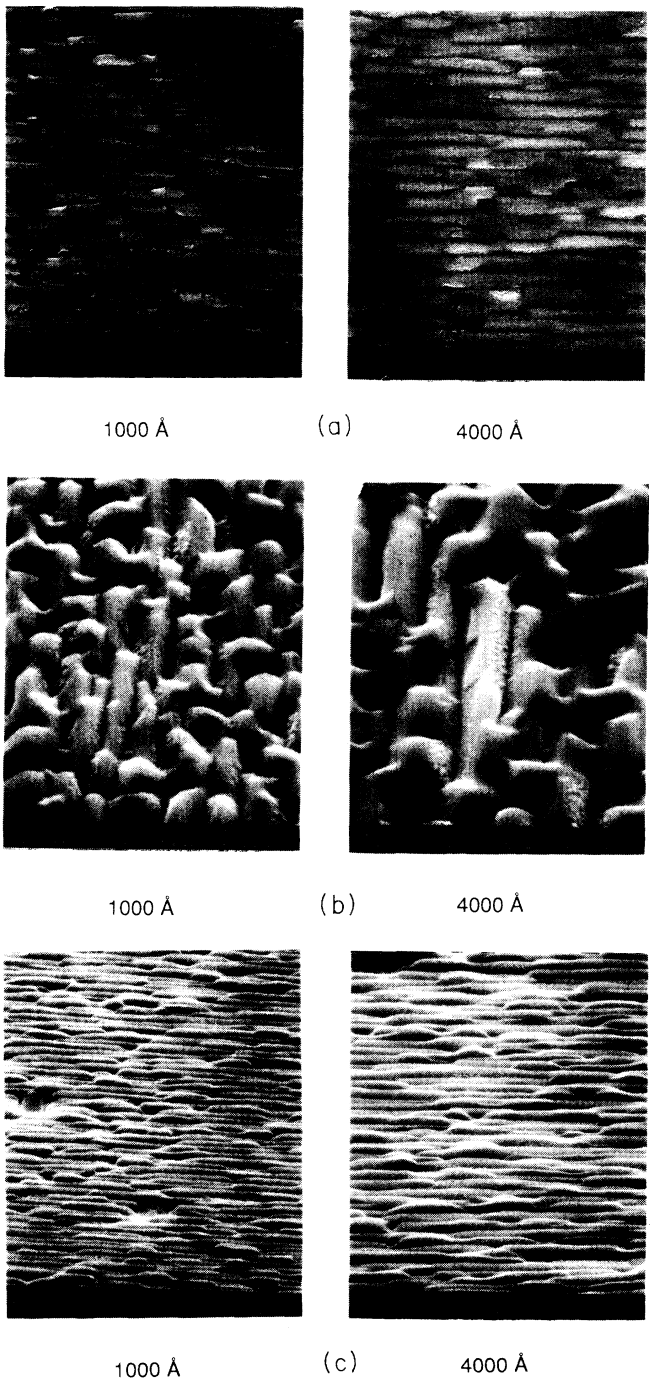

FIG. 2. SEM image of a 1000-Å and 4000-Å-thick (103) oriented YBCO thin film on $LaAlO_3$ (101) substrate. (a) top view, (b) tilted to 60° from the top view along [010] direction, and (c) tilted 60° from the top view along [$\bar{3}$01] direction.

TABLE I. The characteristics of the (103), *c*-axis and *a*-axis oriented YBCO thin films and twinned single crystal along the different in-plane directions.

Substrate	Substrate temp. (°C)	Texture	T_c (K)	$J\|\|$ direction of substrate	$d\rho/dT$ ($\mu\Omega$ cm/K)	$\rho(0)$ ($\mu\Omega$ cm)	ρ_{300} ($\mu\Omega$ cm)	Film thickness (Å)	Grain width (Å)	J_c (A/cm^2)
$LaAlO_3$(101)	720	(103)	88.5	J||[010]	1.07	0	320	1000	1700	
$LaAlO_3$(101)	720	(103)	88.5	J||[$\bar{1}$01]	6.0	1400	3200	1000	1700	
$LaAlO_3$(101)	720	(103)	88.5	J||[010]	0.8	0	240	2000	2500	
$LaAlO_3$(101)	720	(103)	88.5	J||[$\bar{1}$01]	7.16	550	2700	2000	2500	
$LaAlO_3$(101)	720	(103)	87.5	J||[010]	0.58	0	180	4000		
$LaAlO_3$(101)	720	(103)	87.5	J||[010]	7.08	125	2250	4000		
MgO(100)	720	*c*	86.5	J||[010]	0.58	0	180	4000		5×10^7 @4 K
$SrTiO_3$(100)	640	*a*	85	J||[010]	1.1	800	1200	4000		1×10^6 @4 K
Single crystal (Refs. 25 and 26)			90	$J\|\|ab$	0.5	0	150			

are parallel to the [010] direction of the substrate, so we expect high conductivity and critical current densities in this direction. However, for the other planar direction, the macroscopic current flow in the YBCO is along both ⟨301⟩ and ⟨031⟩.

B. Morphology

The surface morphology of the films was investigated by scanning electron microscopy. Figure 2(a) shows SEM micrographs (top view) of a 1000- and 4000-Å-thick YBCO film grown on (101) $LaAlO_3$. All the grains in a film are elongated in the same direction, and have a length-to-width ratio of about 10. X-ray diffraction and TEM were used to establish that the elongation of the YBCO is always along the [010]/[100] direction. As the film thickness is increased, the grains start to coalesce so that, viewed from the top, it would appear that bigger grains are obtained (see also Table I). As expected bigger grains are also obtained at higher growth temperature and lower oxygen pressure due to the higher atomic mobility. We will discuss the grain growth mechanisms in the next section.

Figure 2(b) is a side view of the film, looking into the substrate [010] direction. The cross section of the grains [Fig. 2(b)] is a triangular shape, which will be discussed below. In contrast to the extremely smooth surfaces obtainable in *c*-axis and *a*-axis films,[3,20] our (103) films are not smooth. The surface roughness is around 400 Å in the 660-Å thick film. Figure 2(c) is the other side view, looking into the substrate [$\bar{1}$10] direction.

C. Microstructure

Microstructural characterization using transmission electron microscopy (TEM) shows the structure of the grains and the different types of grain boundaries along the major crystallographic directions. The results can be correlated with the anisotropy of the transport measurements as well as give insight into the growth mechanisms of these films. The films were observed in both plane view and cross section. The details of the TEM sample preparation are reported elsewhere.[23]

Figure 3(a) shows a plane-view micrograph of the 4000-Å thick film along with the large area diffraction pattern confirming the (103) orientation. Diffraction contrast from the grain structure, (110) twins, and second phase precipitates results in a confusing image; Fig. 3(b) is an idealized schematic showing the general shape of the grains and the projected direction of the (110) twin boundaries within the grains as well as the location of second phase precipitates. The grains form in the tetragonal phase regime as either (103) or ($\bar{1}$03) with the CuO_2 planes making an angle of either ±45 degrees with the substrate surface. (110) twins, where the *a* and *b* axes alternate across a (110) plane, form within the grains as a result of the tetragonal-to-orthorhombic phase transformation during cool down; this results in the additional distinct (013) and (0$\bar{1}$3) orientations, as found in the x-ray pattern. As indicated by the SEM images, the grains are elongated in the [010]/[100] (henceforth referred to as [010]) direction which is a fast growth direction. The orthogonal ⟨301⟩,⟨031⟩ (henceforth referred to as [$\bar{3}$01]) direction is an ordering direction for the Y and Ba atoms, similar to the [001] direction and is therefore a slow growth direction. The (110) twin boundaries are at an oblique angle to the film/substrate interface. Note that the formation of these twins during cool down does not change the orientation of the CuO_2 planes. The grain structure is defined by the ±45 degree orientation of the CuO_2 planes and the grain boundaries are all either low-angle boundaries or different types of 90 degree boundaries with respect to these planes.

Several distinct types of these 90 degree boundaries are observed, as shown schematically in Fig. 4. Type A is a 90 degree [010] twist boundary; type B is a 90 degree basal-plane-faced [010] tilt boundary; type C is a 90 degree symmetrical [010] tilt boundary. Type A boundaries are observed along the [010] direction of the 4000-Å thick film. These boundaries can be identified by tilting the planar TEM specimen approximately 45 degrees

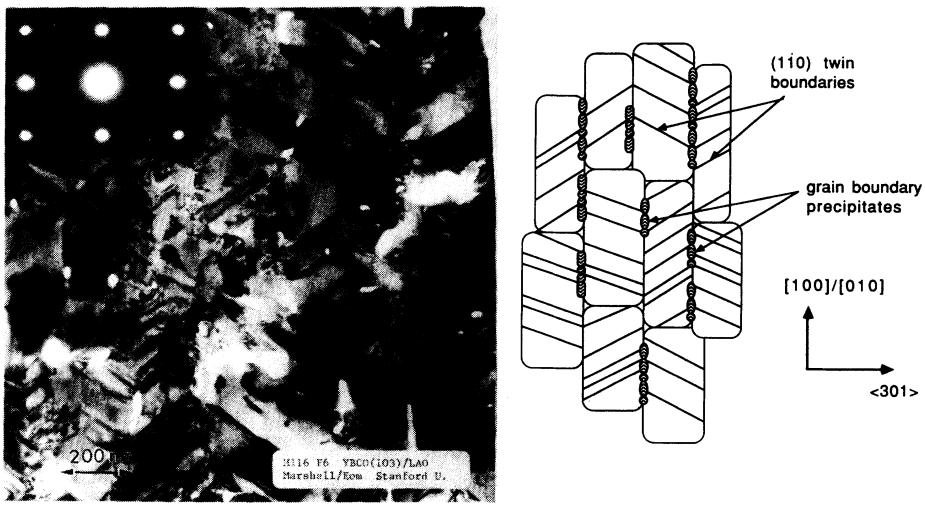

FIG. 3. Planar TEM micrograph (a) and an idealized schematic of the grain and twin boundary structure (b) of a (103) YBCO thin film. The electron diffraction pattern in the inset confirms the in-plane texture and absence of (110) grains.

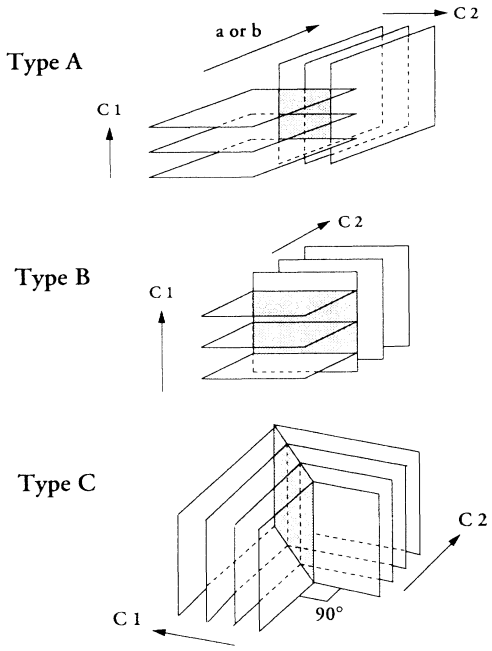

FIG. 4. Schematic diagrams of various 90° grain boundaries; a 90° [010] twist boundary (type A), a 90° [010] basal-plane-faced tilt boundary (type B), and a 90° [010] symmetrical tilt boundary (type C). Note that a 90° [001] tilt boundary is a (110) twin boundary.

about the [010] axis of the film. The type A boundary is then imaged as in Fig. 5, where one is looking along the [001] direction of one grain and along the [100] direction of the other grain, the latter showing the 11.7-Å fringes of the (001) planes. Microdiffraction confirms this orientation change across the boundary. The [010] twist boundaries are the predominant high angle grain boundary along the [010] film direction. Other types of boundaries that occur in this direction are the (110) twin boundaries within the grains, and $c/3$ antiphase boundaries which occur as a result of adjacent grains nucleating in the same orientation but out of registry with each other. Low-angle boundaries may also exist between grains in registry with each other. Finally some of the [010] twist boundaries may also have an *a-b* twin component [similar to the (110) twins], if the [010] and [100] axes alternate across the boundary.

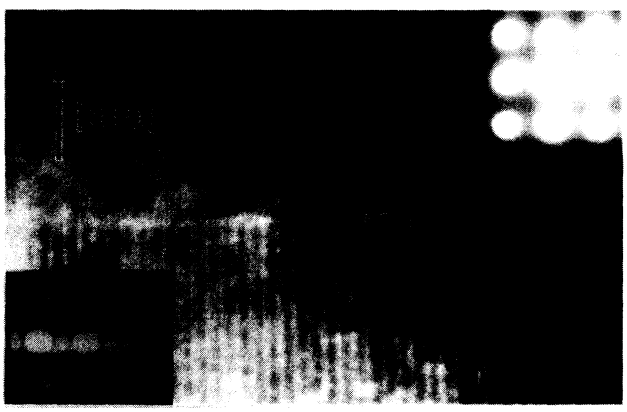

FIG. 5. The 90° [010] twist boundry is shown in Fig. 2(c) in which the sample is rotated 45° about the [010] direction. The *c*-axis fringes of the bottom grain can be seen.

Characterization of the grain growth, and grain boundary structures along the in-plane [$\bar{3}01$] direction are obtained by analyzing a [010] TEM cross-section sample. Figure 6 shows such a cross section of the 660-Å thick film. In contrast to the smooth surfaces of *a*- and *c*-axis film growth,[20] the film surface is very rough. The film does not grow with the (103) plane as the growth front. Rather growth occurs along the [100] and [001] directions, both of which are out of the plane at approximately 45 degrees, resulting in triangular shaped grains. The grain size is very fine at the interface, less than 100 Å. However, as the film thickens, the grains quickly become larger, indicating that the growth rate is much higher than the homogeneous nucleation rate. Both TEM and SEM show the grain size increasing with thickness.

The grain boundaries in the [$\bar{3}01$] direction, as observed in Fig. 6 are type B and type C boundaries (Fig. 4). A perfect type C boundary for a (103) grain has the ($\bar{1}03$) plane as its boundary plane and is expected to be coherent. However many of the boundaries which we observe do not appear perfectly symmetrical or coherent although their boundary plane is very close to ($\bar{1}03$). Further some boundaries are clearly comprised of type B plus type C facets. Since coherent boundaries are energetically favorable, it seems likely that the imperfect type C boundaries are similarly faceted and coherent on a finer scale. This has been reported for grain boundaries in *a*-axis films by Gao *et al.*[11] Twist facets in type-C boundaries have also been identified (see note added in proof). A schematic showing the grain structure and grain boundaries along the major in-plane directions is shown in Figs. 7 and 8.

The cross-section view also gives insight into the nature of film nucleation and growth. (103) film growth is quite different from that of *a*- and *c*-axis growth, in that both the fast [100] and slow [001] growth directions are out of the plane of the substrate at approximately 45 degrees and define the growth fronts for the film. The heterogeneous nucleation rate at the interface is very high, resulting in a grain size of less than 100 Å for the first layer of growth. The grains nucleate in the tetragonal phase regime in one of two orientations, (103) or ($\bar{1}03$), which have a 90 degree relationship of the CuO_2 planes between them. Because the [100] direction is the fast growth direction, two adjacent grains 50-Å apart with these directions intersecting will quickly grow together forming a triangle approximately 50 Å high. Many of these small triangular grains are visible along the film/substrate interface of Fig. 6. Further growth in the [100] directions is blocked by the intersection of the grains and growth then takes place in the kinetically less favored [001] growth direction or by nucleation of a new (100) grain on the (001) surface. However, because we are in the parameter space favoring (001) growth, the nucleation of *a*-axis grains on top of *c*-axis grains is less favorable than grain growth. The areas where *a*-axis nucleation is most favored will be in the valleys where the *c*

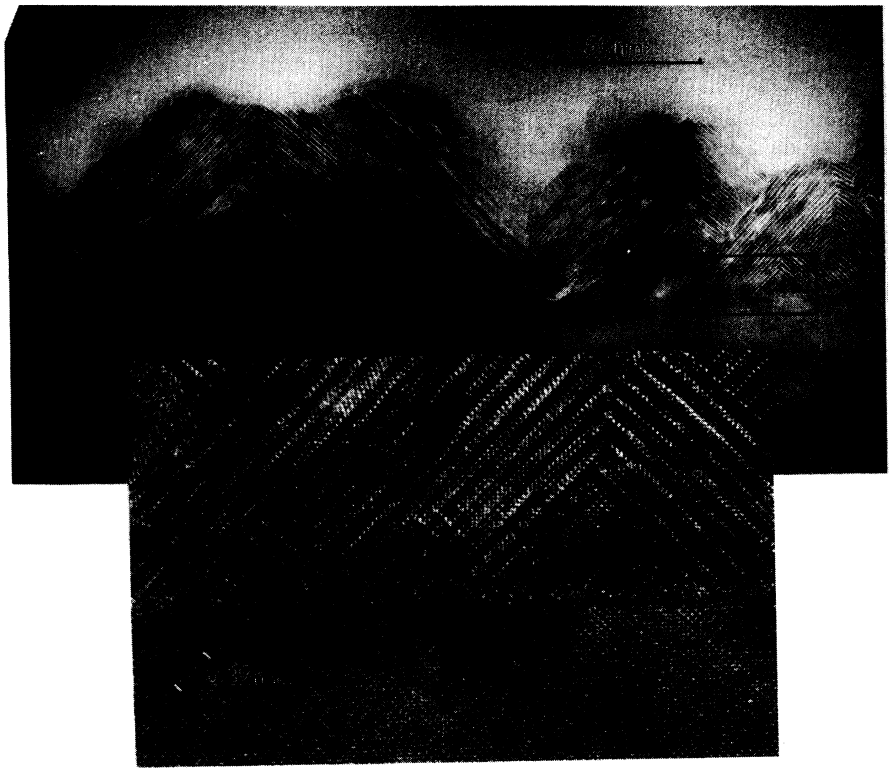

FIG. 6. Low-magnification of 660-Å cross section viewed along substrate [010] direction, showing surface structure, precipitates, grain boundaries. High magnification inset of cross section showing interface grains very clearly.

axes of two grains intersect. Here c-axis growth on one surface may force a-axis growth on the intersecting surface at 90 degrees so that small fluctuations in local growth conditions may favor the type B basal-plane-faced boundary. In the growth regime following the initial copious heterogeneous nucleation at the substrate, many basal-plane-faced type B tilt boundaries are observed in addition to the symmetrical type C tilt boundaries. The grain size increases by a factor of 5–10 times in this regime, supporting the conclusion that grain growth proceeds faster than homogeneous nucleation. It appears that at about 2000 Å nominal film thickness, growth on (001) surfaces at ±45 degrees seems to stabilize and dominate the film structure so that growth beyond this thickness is columnar with (approximately) type C boundaries normal to the plane of the film. As confirmed by planar views of successive thicknesses, the grain size for films thicker than 2000 Å stabilizes at about 2000-Å average width and 2-μm length giving an aspect ratio of about 10. The cross-section view of the 4000-Å thick film does not show sufficient electron transparent area to confirm columnar growth and predominantly type C boundaries above 2000-Å thickness unambiguously, although the planar view of Fig. 3(a), which is the upper 1000 Å of the film, indicates columnar boundaries along the [$\bar{1}$01] substrate direction at this thickness.

The plane view of Fig. 3(a) also shows precipitates on the order of a few hundred angstroms in size in the film, mainly at the grain boundaries in the [$\bar{3}$01] direction. The cross-section view (Fig. 6) shows that the majority of these second phase particles are on the surface of the film, either in the valleys or along the (001) surfaces, suggesting that the extra material is pushed out ahead of the growing 1:2:3 crystal front. Some precipitates are also

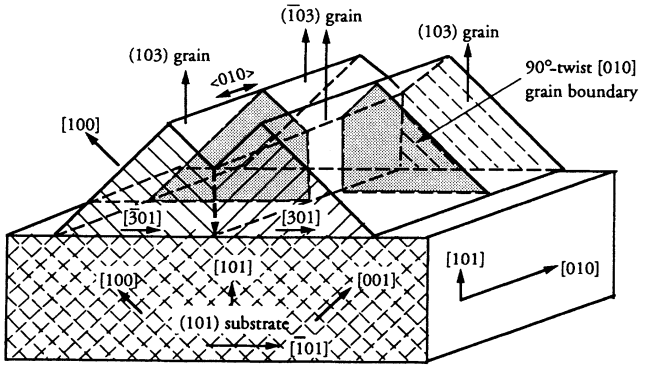

FIG. 7. Three-dimensional schematic diagram of a (103)/($\bar{1}$03) YBCO film showing a 90° [010] twist boundary. The twins are not shown here.

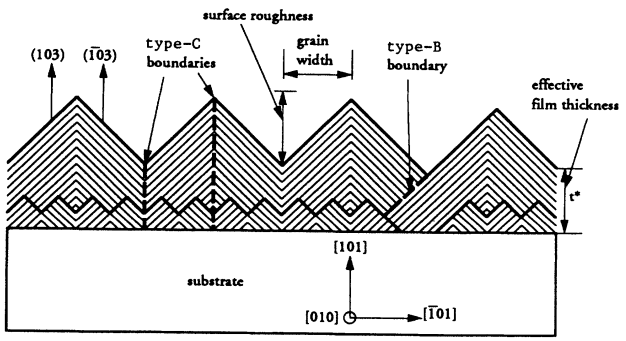

FIG. 8. Schematic cross-section diagram of a (103) film looking into the YBCO [010] directions showing growth kinetics and various boundaries.

embedded in the grain boundaries. These precipitates have been identified as having a cubic lattice with a lattice parameter slightly larger than that of the YBCO sublattice, on the order of 4.1–4.2 Å. Similar precipitates have been identified in Ba-rich evaporated films; these appear to be the insulating "1:3:2" phase as predicted for Ba-rich compositions by the low-pressure phase diagram.[24] The composition of the target used for these films is slightly Ba-rich as determined by inductive coupled plasma spectroscopy so the occurrence of this phase is consistent with phase-diagram considerations. Because these small precipitates are either isolated within the 1:2:3 phase or pushed out to the surface of the film, we do not believe they have a significant effect on the transport properties reported in this paper.

IV. NORMAL AND SUPERCONDUCTING TRANSPORT PROPERTIES

The structure of the (103) film is unique and anisotropic, therefore it is interesting to study its transport properties. We have measured both the normal state properties and superconducting properties of the (103) films with various film thickness from 1000–4000 Å along the two orthogonal directions. As the films become thicker, the microstructure along $[\bar{3}01]$ changes from mixed B+C boundaries near the interface to predominantly C boundaries. We have compared these results with those of the *c*-axis and *a*-axis oriented films. High quality *c*-axis films contain mainly low angle grain boundaries; *a*-axis films contain a mixture of type C and type B grain boundaries.[3] (103) films, as discussed, have type A boundaries in the [010] direction and a combination of types B and C in the $[\bar{3}01]$ direction. In considering types B and C grain boundaries we might intuitively expect better transport properties for type C, since the CuO_2 planes intersect on a roughly one-to-one basis across this boundary. Type B boundaries, on the other hand, have many superconducting planes in one grain intersecting a single plane in the other grain, so that the current path is partially along the *c* axis of the lattice, which is a path of higher resistance. From our results we propose transport mechanisms in the (103) film and fit these with a simple transport model.

A. Resistivity

We have measured resistivity, T_c, and J_c by a four-point measurement. In order to measure the anisotropy, cross-shaped bridges were patterned with two 40-μm lines aligned along the [010] and $[\bar{3}01]$ directions of the (103) YBCO film. For *c*-axis and *a*-axis films these bridge lines were aligned along the [100] and [010] directions of the substrate. Alignment of the bridge along a specific crystallographic orientation is only accurate to within a few degrees; the lack of perfect alignment of the bridges with respect to the grains is a source of small error unless (as is not the case here) one is measuring along the high resistance *c* axis.

Figure 9 shows resistivity vs temperature curves for a 4000-Å thick (103) YBCO film on a (101) $LaAlO_3$ substrate along both the [010] and $[\bar{3}01]$ directions. The resistive transition temperatures (T_c) and transition widths (ΔT_c) along both directions are the same [$T(R=0)=87.5$ K and $\Delta T_c=1.0$ K]. However, the resistivity (ρ) is anisotropic: ρ along the $[\bar{3}01]$ direction is much higher than ρ along the [010] direction. In contrast, in *c*-axis and in *a*-axis films, the resistivity behavior is isotropic in the plane of the film.

The normal state resistivity as a function of temperature can be analyzed, as discussed by Halbritter[25] as

$$\rho_N(T)=\sum_{\text{g.b.}}\rho_{\text{g.b.}}+P(\rho_0^i+\alpha^i T)\ , \tag{1}$$

where $\rho_{\text{g.b.}}$ is the grain boundary resistance; it is assumed

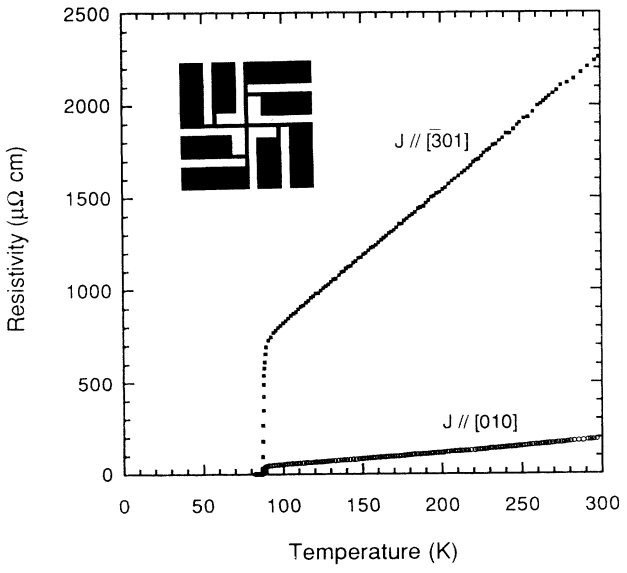

FIG. 9. Resistivity vs temperature curves for a 4000-Å-thick (103) YBCO film on a (101) $LaAlO_3$ substrate along two orthogonal directions. The inset shows the geometry of a cross-shaped-bridge pattern for the transport measurements.

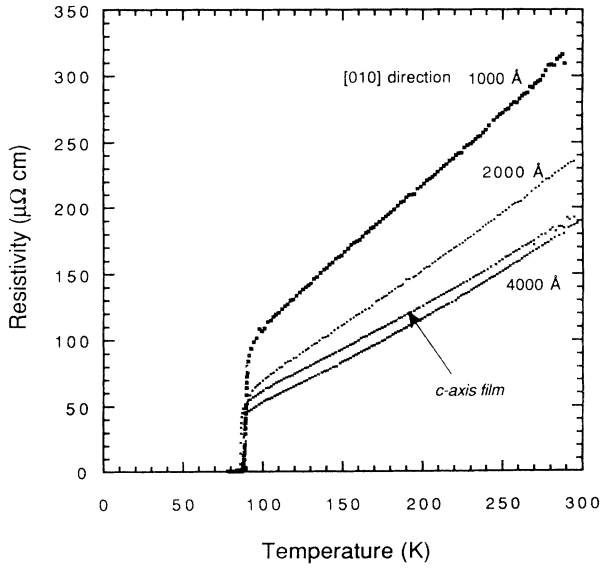

FIG. 10. Resistivity vs temperature curves for 1000-, 2000-, and 4000-Å-thick (103) YBCO films on (101) $LaAlO_3$ substrates along [010] and for a 4000-Å *c*-axis film on a (100) MgO substrate.

to be temperature independent and makes the dominant contribution to $\rho(0)$; $\rho_0^i+\alpha^i T$ is the intrinsic resistance of weak-link-free crystallites; ρ_0^i is impurity scattering, which we assume to be zero as it is in high quality YBCO single crystals; α^i is the intrinsic lattice scattering, and contributes to $d\rho/dT$. For high quality YBCO single crystals $d\rho/dT$ is very close to 0.5 $\mu\Omega$ cm/K;[25,26] and $P=L/L_0\times C_0/C$ is the mean percolative lengthening (L/L_0) and mean shrinkage of the current cross section (C_0/C) and contributes directly to $d\rho/dT$ as indicated.

Figure 10 shows resistivity vs temperature curves for 1000-, 2000-, and 4000-Å-thick (103) YBCO films on (101) $LaAlO_3$ substrates along the [010] direction as well as that of a 4000-Å c-axis film. The transition temperatures of all these films are almost the same, within 1 K.

For the c-axis film, the resistivity behavior along the two orthogonal directions is the same, which is expected since we measure over many a-b twins. The resistivity at room temperature (ρ_{300}) is 195 $\mu\Omega$ cm, the temperature dependence ($d\rho/dT$) is 0.58 $\mu\Omega$ cm/K, and the zero-temperature intercept [$\rho(0)$] is zero. These normal state properties are very close to those of high quality twinned single crystals when $J\|ab$ plane.

For 4000-Å-thick (103) films along the [010] direction, the resistivity [$\rho(T)$] is similar to that of c-axis films. Actually, $\rho(T)$ on (103) films from three different deposition runs with the same film thicknesses is consistently slightly lower than for the c-axis films. The extrapolated intercept gives $\rho(0)\leq 0$. Thus there is no evidence for temperature independent grain boundary resistance due to the presence of the type A [010] twist boundaries.

The [010] resistivity depends on film thickness as can be seen in Table I. $\rho(0)$ always remains close to zero, indicating that there is no grain boundary resistance. However, $d\rho/dT$ increases with decreasing film thickness. For the 100-Å-thick film the value is about twice that of the 4000-Å thick film. We do not expect an increase in path length, since the superconducting planes are parallel to the macroscopic current direction, and the grain boundaries do not show high resistance; therefore, this increase is due to cross-section shrinkage. This may be understood by considering the rough film surfaces and the three-dimensional shape of the grains: Two grains intersecting along the [010] direction may not be exactly aligned, causing reduction of the actual contact area. If one assumes a planar growth front and maximum misalignment for triangular-shaped grains along the [010] direction, the cross-sectional shrinkage is still only on the order of one-half of the total cross-sectional area of individual grains, leading to a factor of 2 maximum increase in $d\rho/dT$. As films thicken, more of the underlying layers make contact, so that the value of the slope approaches the ideal value.

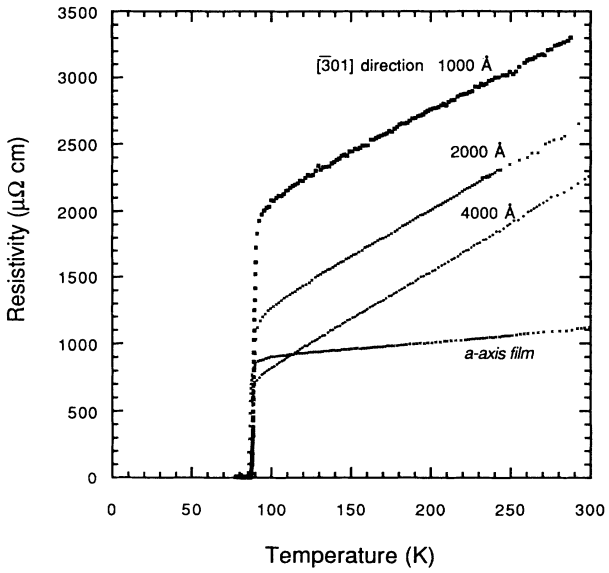

FIG. 11. Resistivity vs temperature curves for 1000-, 2000-, and 4000-Å thick-(103) YBCO films on (101) $LaAlO_3$ substrates along the [$\bar{3}$01] direction and for a 4000-Å a-axis film on a (100) $SrTiO_3$ substrate.

To interpret the transport behavior along the [$\bar{3}$01] direction it is also useful to consider the behavior of a-axis films. The a-axis films have two orientations of the c-axis in-plane; the microscopic current in an a-axis film flows through the CuO_2 planes in a zigzag pattern.[3] As a result, the current path is about twice as long as the direct path, and this current path lengthening increases $d\rho/dT$ by a factor of 2 over that of a c-axis film. $\rho(0)$ is very high because the resistivity of a-axis films is dominated by grain boundary scattering.

Figure 11 shows resistivity vs temperature curves for 1000-, 2000-, and 4000-Å-thick (103) YBCO films on (101) $LaAlO_3$ substrates along the [$\bar{3}$01] direction as well as that of the 4000-Å pure a-axis oriented YBCO film. In both cases type B and C grain boundaries are present. The resistivity behavior of (103) films along the [$\bar{3}$01] direction in which microscopic current also traverses type B and type C boundaries, is very different from that of either c-axis or a-axis films. First, the absolute resistivity is very high. Also, $d\rho/dT$ is about 7 $\mu\Omega$ cm/K, which is about 12 times bigger than that of the c-axis film. This implies that the effect of the microstructure on the current path lengthening and/or the cross-shrinkage is much greater for this direction. We expect both effects from the microstructure shown in Fig. 6. The current paths become longer because the microscopic current flows up and down along the CuO_2 planes. Additionally, if the microscopic current meets a type B grain boundary, which we intuitively expect to have higher resistance, the current direction may change to go through a type C grain boundary into a neighboring grain, which also increases the path length.

Also, we expect a large reduction in cross section due to the surface roughness. Thin regions, or valleys, exist between the triangular shaped grains in the [$\bar{3}$01] direction, as observed in the SEM and cross-section TEM images, and will restrict the current flows. Figure 7 shows that the height of the valleys may be a small fraction of the nominal film thickness; from this observation we would expect cross-section shrinkage to be the dominant contribution to the large value of $d\rho/dT$ in the [$\bar{3}$01] direction. However, it is interesting to note that the value of the slope remains constant as the film thickness varies from 1000 to 4000 Å, suggesting that C_0/C also

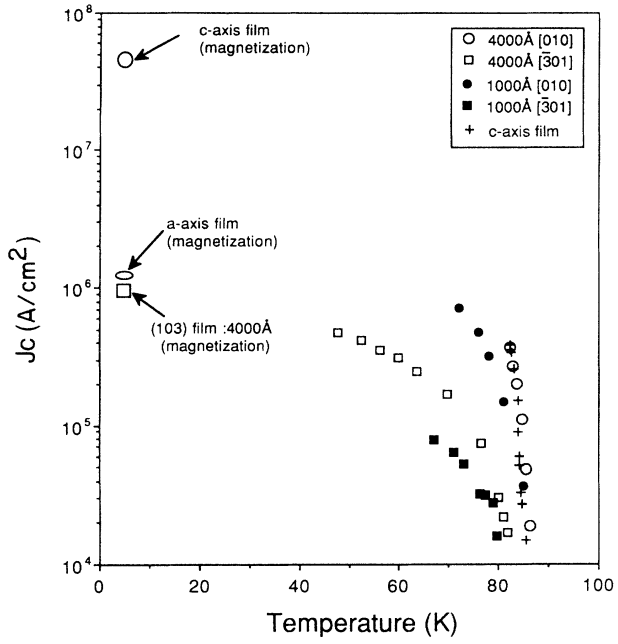

FIG. 12. Critical current density vs temperature curves for a c-axis film and for 1000-Å and 4000-Å-thick (103) films along the two in-plane directions measured by transport. The J_c's at 4.2 K were measured by magnetization at near zero field. The intragrain J_c of a flux grown single crystal [Babcock (Ref. 14)] is 50 times lower than the J_c of the 4000 Å thick (103) film in the [$\bar{3}$01] direction and 3 orders of magnitude lower than the J_c of the c-axis film.

remains constant with thickness. It is not clear that this is due to surface roughness alone since one might expect C_0/C to decrease as the film increases in thickness. The C_0/C factor may be influenced by other microstructural considerations as well. For example, if the type C boundaries, which become more prevalent in the thicker regions of the film, have better transport properties as proposed, then the effective cross section may shift toward upper areas of the film as thickness increases, excluding the lower, more highly resistive regions, and maintaining a constant C_0/C for this range of thickness. This is also consistent with the lower $\rho(0)$ of the thicker films.

B. Critical current densities

Because there are several specific types of boundaries in the (103) film, it is interesting to measure the critical current densities along both orthogonal directions and to compare them with those of c-axis and a-axis films, which are well known. Critical current densities of (103) films have been measured both by transport on 40-μm-wide patterned bridges, and, when was convenient, by the dc magnetization method. The two methods are quite self-consistent. The criteria for the transport J_c was 5 μV/cm. The magnetization J_c was done at 4.2 K at zero field using the Bean approximation.[27]

Figure 12 shows the J_c vs T curves for previously measured c-axis and a-axis films along with 4000- and 1000-Å-thick (103) films measured by transport in the two in-plane directions. The transport J_c of 4000-Å-thick (103) film along the [010] direction is, within experimental error, the same as that of the c-axis film. The transport J_c measurements are near T_c because the maximum current used was limited to 100 mA. Therefore, we conclude that the 90° twist grain boundaries between (103) and ($\bar{1}$03) grains along the [010] direction show no weak link behavior. This unexpected result can be explained in the following way. The type A (Fig. 4) twist is particularly robust in so far as transport is concerned. Across these boundaries, a single CuO_2 plane in each grain makes contact with many CuO_2 planes in the other grain. It is interesting that the 90° twist boundaries may actually improve transport properties by shorting out defects such as stacking faults. This allows for transport without having to travel along the highly resistive c axis. The 90° [010] twist boundary also may be advantageous in situations where electrical contact is made only to a surface layer. Although there is some antisite cation disorder between Ba and Y across the 90° twist boundary the common copper and oxygen atoms positions are unaltered.

The J_c of 4000-Å thick (103) films along the [$\bar{3}$01] direction, however, is about 30 times lower than along the [010] direction. This measurement is affected not only by the grain boundary structure along this direction, but also by the cross-section shrinkage effect indicated by the normal state resistivity measurements. As discussed, $d\rho/dT$ is a factor of 12 larger than that of the c-axis film or of the (103) film along the [010] direction. Current path lengthening due to the zigzag microscopic current along the CuO_2 planes can contribute to higher $d\rho/dT$ by a factor of $\sqrt{2}$; therefore we expect a reduction in ρ due to cross-sectional shrinkage by up to a factor of 9.

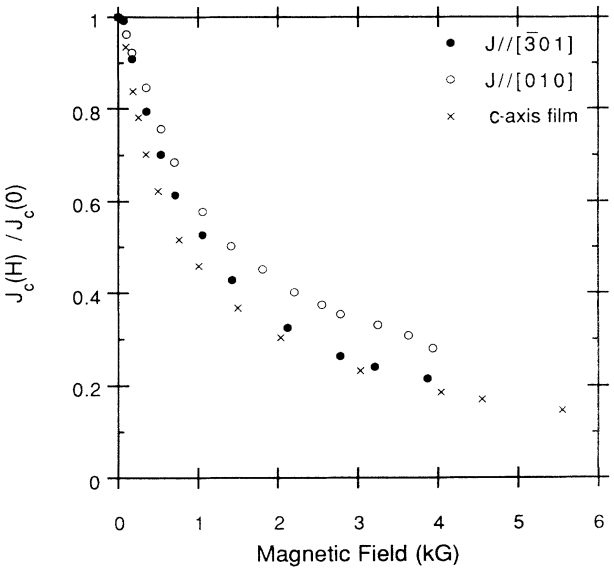

FIG. 13. Normalized critical current density $[J_c(H)/J_c(0)]$ as a function of magnetic field for a 4000-Å-thick (103) YBCO film on a (101) $LaAlO_3$ substrate along two orthogonal directions and for a 4000-Å c-axis film on a (100) MgO substrate. The effective magnetic field in the (103) film is $1/\sqrt{2}$ because the CuO_2 planes are at 45° at the substrate surface. All three data sets show very similar magnetic field dependence.

This factor is an upper limit since we cannot determine what other path lengthening effects may also contribute to the resistivity slope. If we apply this same cross-section shrinkage in determining J_c, then the true value of J_c in the $[\bar{3}01]$ direction is up to 9 times higher than that shown in Fig. 13. The remainder of the difference between $J_c[\bar{3}01]$, and $J_c[010]$ and that of the c-axis films, is due to the effect of grain boundaries.

Comparing the behavior of a-axis films, which also contain both type B and C boundaries, may give further insight into the effect of these boundaries on J_c. The J_c of these a-axis films, measured by magnetization, is 1×10^6 A/cm^2. The same measurement for the (103) films will lie between that of the a-axis and c-axis films, if one includes the factor for cross-section shrinkage as discussed in the previous paragraph. This difference between films with the same types of grain boundaries may be explained by considering the details of the microstructure and assuming that the B boundaries are more detrimental to J_c than the C boundaries. For the a-axis films the two types of boundaries are always measured in series. The J_c measurement will therefore reflect the more detrimental boundary. However, for the (103) films there should be a parallel path which traverses only C boundaries in the upper region of the film. This has the effect of increasing the overall J_c relative to that of the a-axis films as observed. This microstructural explanation is consistent with the interpretation of the normal state resistivity behavior for the (103) films.

The J_c's of the (103) films also vary with thickness in both the [010] and the $[\bar{3}01]$ directions as shown in Fig. 12. In the [010] direction, as with the normal state resistivity behavior, this is mainly due to cross-sectional shrinkage for the 1000-Å-thick film. However, in the $[\bar{3}01]$ direction the lower J_c for the thinner film is not due to cross-sectional shrinkage because C_0/C stays constant with thickness as indicated by the resistivity measurements (see Table I). Rather we suggest that the reduction in J_c is due to the variation in boundary structure with thickness. As we discussed we can observe more type B boundaries near the substrate-film interface (see Fig. 7). We attribute the lower J_c's for the thin (103) films to the presence of these boundaries. However, with increasing film thickness, the type C boundaries are more dominant; therefore, J_c increases with thickness. We conclude from both the J_c and resistivity measurements, correlated with the microstructural observations, that the type B boundary is more detrimental to J_c than the (approximately) type C boundary.

The lower J_c and higher $\rho(0)$ both of the (103) films in the $[\bar{3}01]$ direction and of the a-axis film, suggest that these grain boundaries may exhibit weak-link behavior (i.e., strong dependence of J_c on weak magnetic fields). In order to check this we have measured transport J_c's at 77 K as a function of magnetic field up to 5 kG. If weak-link behavior exists we expect to see a rapid drop of J_c at low magnetic field. Figure 13 shows the normalized critical current densities $[J_c(H)/J_c(0)]$ as a function of magnetic field for 4000-Å-thick (103) YBCO films on (101) $LaAlO_3$ substrates along the two orthogonal directions, and for a 4000-Å c-axis film on (100) MgO substrate. The direction of the applied magnetic field is always perpendicular to the substrate surface. Studies[28] of the dependence of J_c on magnetic field orientation in (001)-textured films suggest that for $0<\theta<60°$ the critical current is affected only by the component of the field in the plane. Therefore, the effective magnetic field in the (103) film is reduced by a factor of $\cos(45°)=1/\sqrt{2}$ because the CuO_2 planes are included at 45° to the substrate surface. With this factor taken into account, a very similar field dependence is observed in all three cases, as shown in Fig. 13. In the [010] direction this is as expected since we are measuring across the 90° [010] twist boundaries, which from our previous discussion are not expected to be weak links. However, this is a surprising result for the $[\bar{3}01]$ direction which traverses a mixture of type B and type C 90° tilt boundaries (see, however, note added in proof). Magnetization measurements on a-axis films with a vibrating sample magnetometer are consistent in that the hysteresis loops can be scaled to those of c-axis films.[29]

For current flowing in the $[\bar{3}01]$ direction, then, the inferred magnitude of J_c is ~fourfold smaller than the in-plane critical current of a c-axis film, while the field dependence is almost identical. Should the former behavior be described as weak-link behavior? The distinction between bulk pinning-limited behavior (as in a c-axis film) and weak-link behavior is blurred in the present circumstances. Any connecting region where the order parameter is reduced from its bulk value may be called a weak link, yet the critical current of the system may be limited by bulk pinning rather than the weak link itself, and this would not be called "weak link behavior." In the present case we do not know if J_c in the $[\bar{3}01]$ direction is reduced in comparison to a c-axis film because the former has weaker bulk pinning (due, e.g., to a different defect structure) or because the order parameter is reduced at the 90° boundaries (perhaps leading to a lower pinning force there). The field dependence is also not definitive. A weak link at a type B tilt boundary which had a critical current of 10^6 A/cm^2 would have a characteristic field for the reduction of J_c of $H\sim\phi_0/\lambda_J(\lambda_c+\lambda_{ab})\sim1$ kOe—just

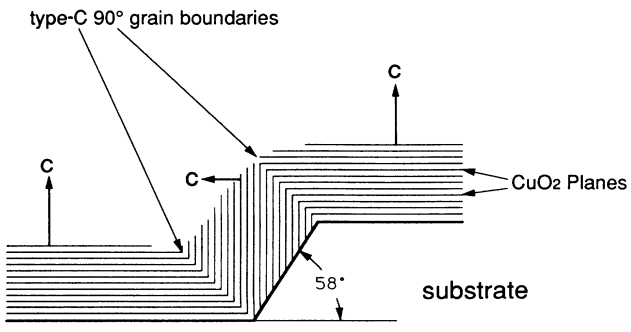

FIG. 14. Schematic cross-section diagram of a step-edge junction showing type C 90° grain boundaries. This figure is drawn based on a cross-sectional TEM micrograph of a step-edge junction investigated by Jia *et al.* (Ref. 17).

as measured. But we see from the data on the *c*-axis film that this is also the characteristic field for decrease in the bulk pinning-dominated critical current.

In a practical sense the nomenclature is unimportant. What we expected was to find a clear indication of weak-link behavior, comparable to that seen in step-edge Josephson junctions[16–18] with high step angles, which incorporate 90° grain boundaries at each level (see Fig. 14). These junctions have critical current in the range 10^3–10^4 A/cm^2, and the critical current decreases in characteristic field in the range 10–100 Oe. Our results demonstrate that such weak coupling is not due to the simple presence of 90° boundaries. Jia *et al.*[30] have demonstrated that there are additional defects associated with the boundaries, which might include compositional variations, strain, or microcracks. These defects either independently or in conjunction with the grain boundaries would seem to be responsible for the weak-link behavior. The consistency of the results for step-edge junctions indicates that such defects would have to occur reproducibly, which may seem unlikely. Another possibility is that the behavior is caused by conduction along the *c* axis, which is inherent in this step geometry for a sufficiently thin film (see Fig. 14). In any case, we have clearly demonstrated that the 90° *c*-axis boundaries need not exhibit significant weak-link behavior.

V. SUMMARY AND CONCLUSIONS

We have grown (103) oriented YBCO films on (101) oriented $SrTiO_3$ and $LaAlO_3$ substrates *in situ* by 90° off-axis sputtering and studied the growth mechanisms, microstructure, anisotropic transport properties and properties of various 90° *c*-axis grain boundaries of the films. The film growth is three dimensional, i.e., the (103) plane is not the growth front. Consequently the film surfaces are very rough, in contrast to *a*- and *c*-axis films. This growth process produces a unique anisotropic microstructure. A domain structure exists with the CuO_2 planes oriented at ±45° to the substrate surface resulting in specific types of 90° grain boundaries along the two orthogonal directions in the film. The anisotropic transport behavior along the two major in-plane directions is explained by the microstructure and a simple transport model. The normal state conductivity, critical current density, and the magnetic field dependence of J_c across 90° [010] twist boundaries is similar to high quality *c*-axis oriented films. The conductivity and critical current density across the 90° tilt boundaries in the [$\bar{3}$01] direction are much lower than in the [010] direction. Most of the discrepancy is accounted for by the reduced effective cross section in this direction. The remainder is attributed to the presence of Type B boundaries (Fig. 4). However, the scaling of J_c with magnetic field for directions traversing type B and C boundaries is the same as for those crossing type A boundaries and as for *c*-axis films with no high-angle boundaries. The weak-link behavior observed by others in step-edge junctions cannot be attributed solely to the 90° boundary misorientation that they contain, because we have demonstrated similar grain boundaries with very strong coupling across the boundary.

Note added in proof. Recent high-resolution microscopy of (approximately) type-C boundaries in the upper regions of (103) films indicates that, in addition to type-B facets already mentioned, these boundaries may also contain nanoscale 90° twist facets, on the order of 10–30 Å in size. The boundary structure is therefore more complicated on the scale of a few nanometers than the ideal symmetrical type-C boundary shown in Fig. 4. Since the type-A twist boundaries do not degrade J_c, these twist facets may be responsible for the non-weak-link behavior indicated by the magnetic-field dependence of J_c along the [$\bar{3}$01] direction. Such an interpretation leaves the charactreistics of the perfectly symmetrical type-C boundary uncertain.

ACKNOWLEDGMENTS

We thank R. W. Simon for the initial SEM work on our (103) film done at TRW. We also would like to thank S. S. Laderman, J.-M. Triscone, and J. Halbritter for helpful discussions. The work at Stanford has been supported in part by AFOSR under Contract Nos. F49620-88-C-004 and F49620-88-C-001, by EPRI, and by the Stanford Center for Materials Research under the NSF-MRL program.

*Present address: AT&T Bell Laboratories, Murray Hill, New Jersey 07974.

[1]S. W. Tozer *et al.*, Phys. Rev. Lett. **59**, 1768 (1987).

[2]T. K. Worthington, W. J. Gallagher, and T. R. Dinger, Phys. Rev. Lett. **59**, 1160 (1987).

[3]C. B. Eom, A. F. Marshall, S. S. Laderman, R. D. Jacowitz, and T. H. Geballe, Science **249**, 1549 (1990).

[4]A. Inam *et al.*, Appl. Phys. Lett. **57**, 2484 (1990).

[5]Due to transformation twins and symmetry considerations the film orientations are not fully described by a single plane, e.g., so-called "(103)" films actually contain (103), ($\bar{1}$03), (013), and (0$\bar{1}$3) orientations. For simplicity we will use the single plane and direction notations, and will not distinguish the *a* and *b* axes or crystallographically equivalent planes, except where necessary in describing boundary structures.

[6]T. Terashima, Y. Bando, K. Iijima, K. Yamamoto, and K. Hirata, Appl. Phys. Lett. **53**, 2232 (1988).

[7]E. Olsson, A. Gupta, M. D. Thouless, A. Segmuller, and D. R. Clarke, Appl. Phys. Lett. **58**, 1682 (1991).

[8]Osamu Wada *et al.* Jpn. J. Appl. Phys. **30**, L722 (1991).

[9]Osamu Wada *et al.* Jpn. J. Appl. Phys. **30**, L1181 (1991).

[10]J. Kwo, R. M. Fleming, H. L. Kao, D. J. Werder, and C. H. Chen (unpublished).

[11]Y. Gao, G. Bai, D. J. Lam and K. L. Merkle, Physica C **173**, 487 (1991).

[12]D. Dimos, P. Chaudhari, and J. Mannhart, Phys. Rev. B **41**, 4038 (1990).

[13]Z. G. Ivanov, P. A. Nilsson, D. Winkler, J. A. Alarco, T. Claeson, E. A. Stepantsov, and A. Ya. Tzalenchuk, Appl. Phys. Lett. **59**, 3030 (1991).

[14]S. E. Babcock, X. Y. Cai, D. L. Kaiser, and D. C. Labalestier, Nature (London) **347**, 167 (1990).

[15]C. B. Eom, A. F. Marshall, Y. Suzuki, B. Boyer, R. F. W. Pease, and T. H. Geballe, Nature (London) **353**, 544 (1991).
[16]K. P. Daly, W. D. Dozier, J. F. Burch, S. B. Coons, R. Hu, C. E. Platt, and R. W. Simon, Appl. Phys. Lett. **56**, 785 (1990).
[17]C. L. Jia, B. Kabius, K. Urban, K. Herrmann, G. J. Cui, J. Schubert, W. Zander, A. I. Braginski, and C. Heiden, Physica C **175**, 545 (1991).
[18]K. Herrmann, Y. Zhang, H.-M. Muck, J. Schubert, W. Zander, and A. I. Braginski, Superconductor Sci. Technol. **4**, 583 (1991).
[19]C. B. Eom *et al.*, Appl. Phys. Lett. **55**, 595 (1989).
[20]C. B. Eom *et al.*, Physica C **171**, 351 (1990).
[21]C. B. Eom, A. F. Marshall, J.-M. Triscone, B. Wilkens, S. S. Laderman, and T. H. Geballe, Science **251**, 780 (1991).
[22]K. Char *et al.*, Appl. Phys. Lett. **56**, 785 (1990).
[23]A. F. Marshall *et al.*, J. Mater. Res. **5**, 2049 (1990).
[24]B. T. Ahn *et al.*, Physica C **167**, 529 (1990).
[25]J. Halbritter, Int. J. Mod. Phys. B **3**, 719 (1989).
[26]S. J. Hagen, T. W. Jing, Z. Z. Wang, J. Horvath, and N. P. Ong, Phys. Rev. B **37**, 7928 (1988).
[27]C. P. Bean, Phys. Rev. Lett. **54**, 1702 (1962).
[28]R. B. van Dover (private communication).
[29]C. B. Eom *et al.* (unpublished).
[30]C. L. Jia, B. Kabius, K. Urban, K. Herrmann, J. Schubert, W. Zander, and A. I. Braginski (unpublished).

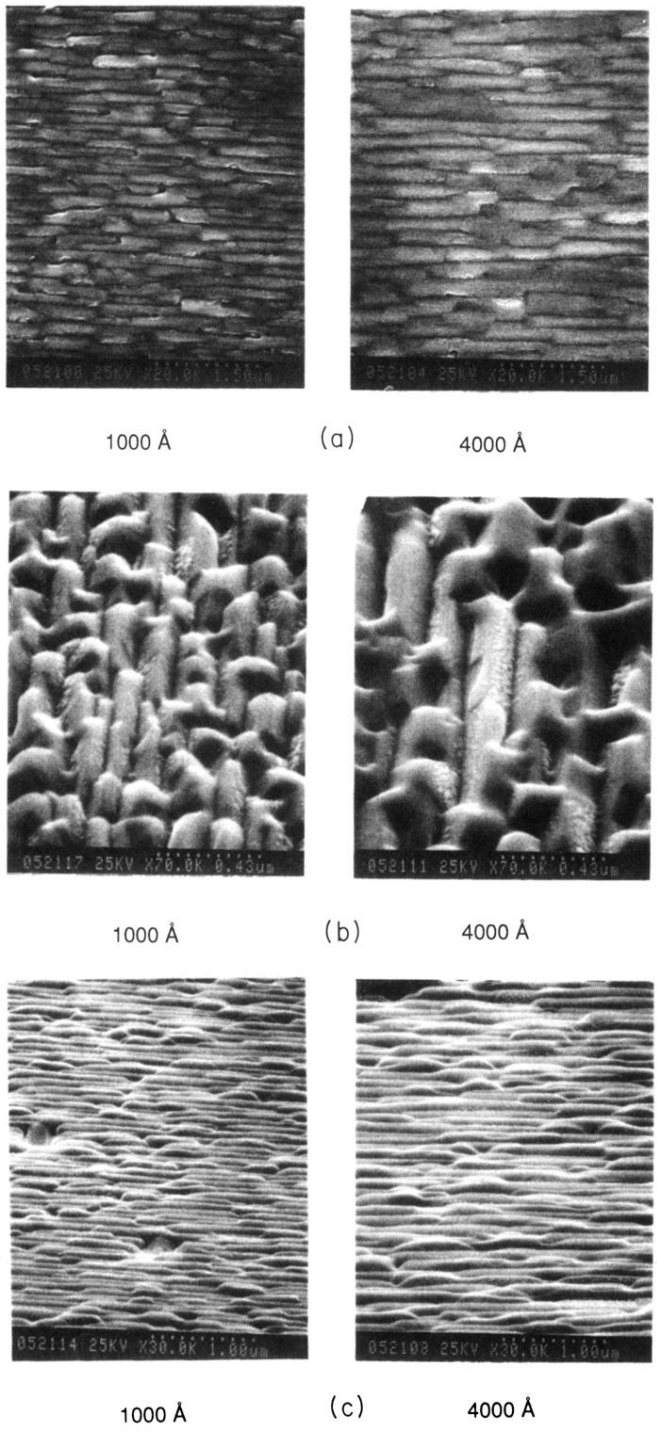

FIG. 2. SEM image of a 1000-Å and 4000-Å-thick (103) oriented YBCO thin film on $LaAlO_3$ (101) substrate. (a) top view, (b) tilted to 60° from the top view along [010] direction, and (c) tilted 60° from the top view along $[\bar{3}01]$ direction.

(a)

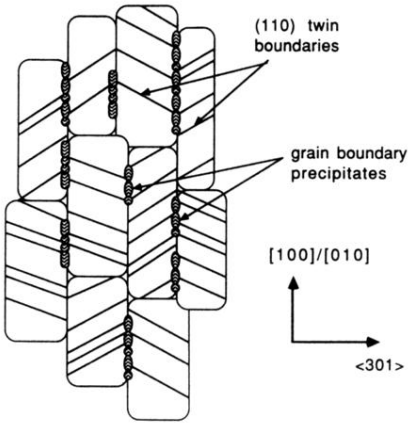

(b)

FIG. 3. Planar TEM micrograph (a) and an idealized schematic of the grain and twin boundary structure (b) of a (103) YBCO thin film. The electron diffraction pattern in the inset confirms the in-plane texture and absence of (110) grains.

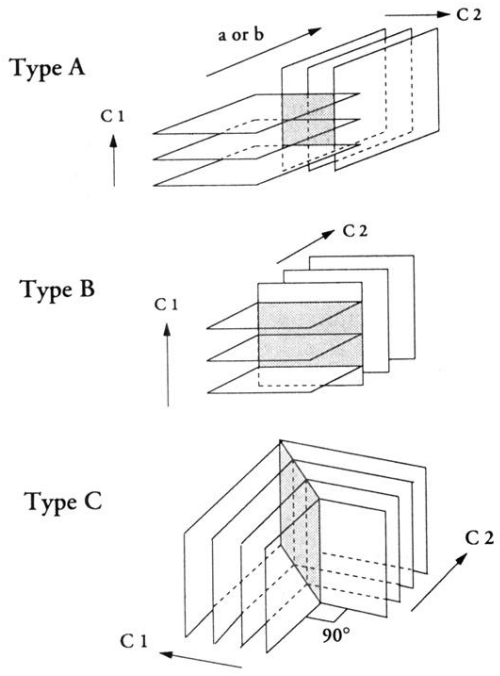

FIG. 4. Schematic diagrams of various 90° grain boundaries; a 90° [010] twist boundary (type A), a 90° [010] basal-plane-faced tilt boundary (type B), and a 90° [010] symmetrical tilt boundary (type C). Note that a 90° [001] tilt boundary is a (110) twin boundary.

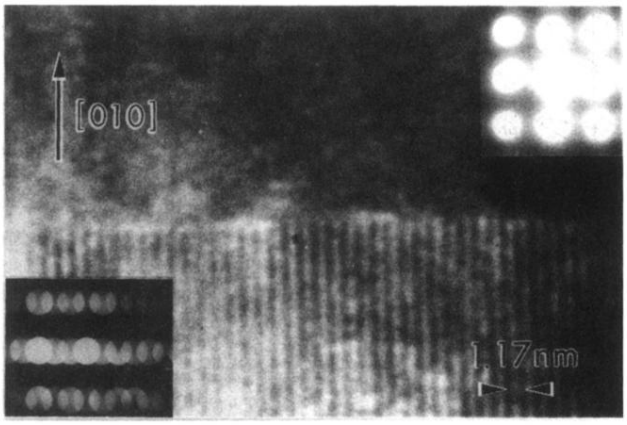

FIG. 5. The 90° [010] twist boundry is shown in Fig. 2(c) in which the sample is rotated 45° about the [010] direction. The *c*-axis fringes of the bottom grain can be seen.

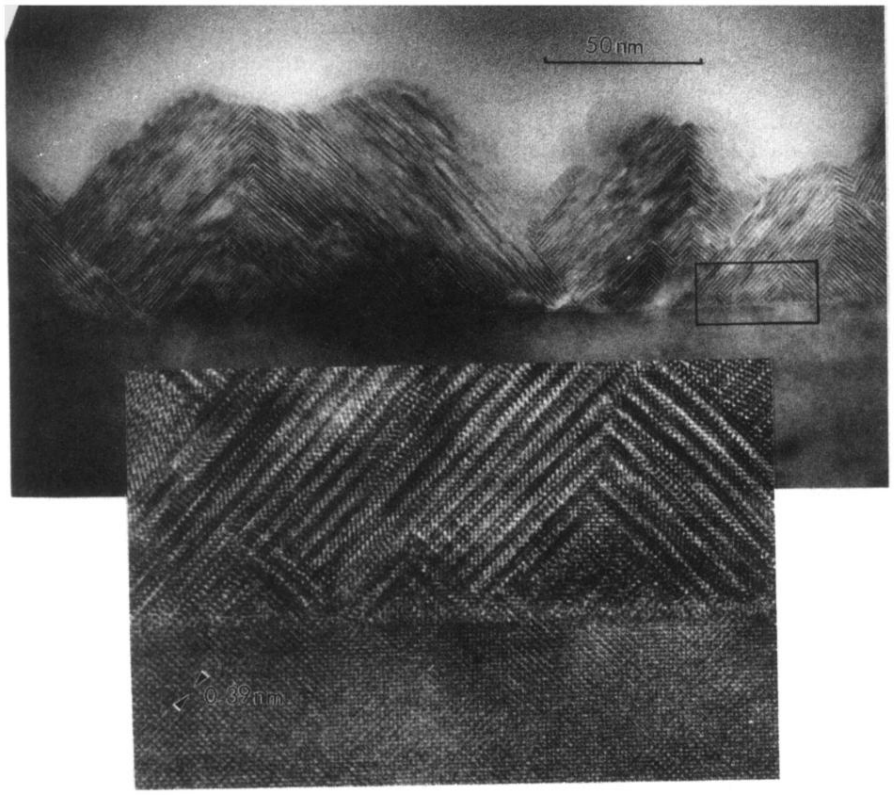

FIG. 6. Low-magnification of 660-Å cross section viewed along substrate [010] direction, showing surface structure, precipitates, grain boundaries. High magnification inset of cross section showing interface grains very clearly.

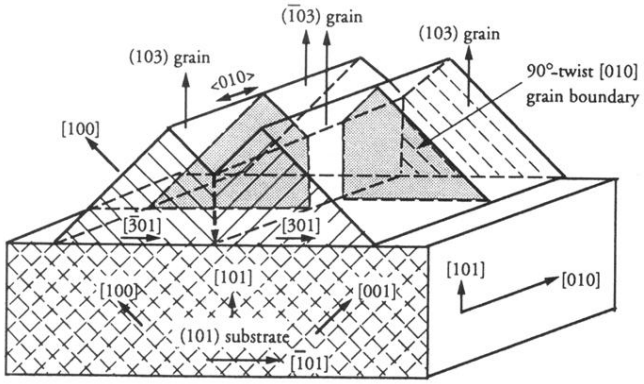

FIG. 7. Three-dimensional schematic diagram of a (103)/(1̄03) YBCO film showing a 90° [010] twist boundary. The twins are not shown here.